Lab on a Chip

Cite this: *Lab Chip*, 2011, **11**, 645

www.rsc.org/loc

PAPER

Suspended microchannel resonators with piezoresistive sensors

J. Lee,†[ab] R. Chunara,†[c] W. Shen,[d] K. Payer,[e] K. Babcock,[f] T. P. Burg[g] and S. R. Manalis*[ah]

Received 26th September 2010, Accepted 1st December 2010
DOI: 10.1039/c0lc00447b

Precision frequency detection has enabled the suspended microchannel resonator (SMR) to weigh single living cells, single nanoparticles, and adsorbed protein layers in fluid. To date, the SMR resonance frequency has been determined optically, which requires the use of an external laser and photodiode and cannot be easily arrayed for multiplexed measurements. Here we demonstrate the first electronic detection of SMR resonance frequency by fabricating piezoresistive sensors using ion implantation into single crystal silicon resonators. To validate the piezoresistive SMR, buoyant mass histograms of budding yeast cells and a mixture of 1.6, 2.0, 2.5, and 3.0 μm diameter polystyrene beads are measured. For SMRs designed to weigh micron-sized particles and cells, the mass resolution achieved with piezoresistive detection (~3.4 fg in a 1 kHz bandwidth) is comparable to what can be achieved by the conventional optical-lever detector. Eliminating the need for expensive and delicate optical components will enable new uses for the SMR in both multiplexed and field deployable applications.

1. Introduction

In addition to being central to the field of scanning probe microscopy, the use of microcantilevers has led to high precision methods for detecting biomolecules,[1–5] viruses,[6] and cells.[7,8] Microcantilever deflection is conventionally measured by a technique known as the optical-lever wherein a laser beam is reflected off the cantilever onto a position sensitive photodiode.[9,10] The optical-lever is sensitive and straightforward to implement but requires well-aligned external optical components. Piezoresistive sensors eliminate the need for external components by enabling measurement of deflection through the resistance change of a sensing element integrated onto the cantilever.[11]

In the recently developed suspended microchannel resonator (SMR), microfluidic channels are incorporated inside a microcantilever resonator, which significantly reduces viscous damping from fluid and allows buoyant mass to be measured with high resolution. Single nanoparticles, single cells, and submonolayers of adsorbed proteins have previously been weighed in fluid environments using the SMR with optical-lever detection.[12,13] For the laboratory setting wherein only one or two SMRs are used at the same time, optical-lever detection has not limited overall performance. Although optical detection schemes have successfully been used for parallel readout of micro- and nanocantilevers,[14–16] our intent here is to evaluate the performance of piezoresistive detection for measurements that require dense arrays of SMRs or for field deployable applications wherein maintaining the alignment would be difficult. In light of this, we have developed piezoresistive SMRs with single crystal silicon *via* ion implantation and have evaluated their performance for weighing single particles and cells. Two designs were fabricated: one with a cantilever length of 210 μm and a resonance frequency of ~347 kHz and the other with a cantilever length of 406 μm and a resonance frequency of ~92 kHz (see Table 1 for other dimensions and characteristics). The mass resolution for a particle at the tip in a 1 kHz bandwidth achieved by the piezoresistive detection was approximately 3.4 and 18.1 fg for 210 and 406 μm long SMRs, respectively. Piezoresistive detection was approximately 21% less and 30% more sensitive than optical detection for the 210 and 406 μm long SMRs, respectively.

2. Device fabrication

Many types of transducers have incorporated piezoresistive detection, including pressure sensors[17,18] and accelerometers.[19] Piezoresistors have been previously implemented with doped semiconducting materials or thin film metals and have been

[a]*Department of Biological Engineering, Massachusetts Institute of Technology, Cambridge, MA, 02139, USA. E-mail: scottm@media.mit.edu; Fax: +1-617-253-5102; Tel: +1-617-253-5039*
[b]*Current address: Department of Mechanical Engineering, Sogang University, Seoul, 121-742, Korea*
[c]*Harvard-MIT Division of Health Sciences and Technology, Massachusetts Institute of Technology, Cambridge, MA, 02139, USA*
[d]*Innovative Micro Technology, Santa Barbara, CA, 93117, USA*
[e]*Microsystems Technology Laboratories, Massachusetts Institute of Technology, Cambridge, MA, 02139, USA*
[f]*Affinity Biosensors, Santa Barbara, CA, 93117, USA*
[g]*Max Planck Institute for Biophysical Chemistry, 37077 Göttingen, Germany*
[h]*Koch Institute for Integrative Cancer Research, Massachusetts Institute of Technology, Cambridge, MA, 02139, USA*
† These authors contributed equally to this work.

Table 1 Dimensions, characterization results, and comparison between optical-lever detection and piezoresistive detection

	Characteristics	210 μm SMR	406 μm SMR
Dimensions	Resonator width	28.5 μm	28.5 μm
	Resonator thickness	12 μm	12 μm
	Channel width	7.9 μm	7.9 μm
	Channel height	8 μm	8 μm
	Piezoresistor length	105 μm	105 μm
	Piezoresistor width	3.94 μm	3.94 μm
Common	Resonance frequency (wet)	346.6 kHz	92.1 kHz
	Quality factor (wet)	3700	10 850
	Spring constant (dry)[a]	190.8 N m^{-1}	26.3 N m^{-1}
	Mass sensitivity	−5.42 Hz pg^{-1}	−0.74 Hz pg^{-1}
	Mass sensitivity[a]	−5.62 Hz pg^{-1}	−0.79 Hz pg^{-1}
Optical-lever detection	Frequency noise (BW = 1 kHz)[b]	15.3 mHz (44 ppb)	19.1 mHz (207 ppb)
	Mass resolution (BW = 1 kHz)	2.8 fg	25.8 fg
	Max. ΔT (120 μW, 3% of 4 mW)[a]	0.80 °C	1.62 °C
	Avg. ΔT (120 μW, 3% of 4 mW)[a]	0.45 °C	0.90 °C
	Displacement noise	0.2 pm/$\sqrt{\text{Hz}}$	0.8 pm/$\sqrt{\text{Hz}}$
Piezoresistive detection	Frequency noise (BW = 1 kHz)[b]	18.5 mHz (54 ppb)	13.4 mHz (146 ppb)
	Mass resolution (BW = 1 kHz)	3.4 fg	18.1 fg
	Max. ΔT (125 μW @ 5 V)[a]	0.33 °C	0.33 °C
	Avg. ΔT (125 μW @ 5 V)[a]	0.27 °C	0.30 °C
	Displacement noise[c]	72 pm/$\sqrt{\text{Hz}}$	29 pm/$\sqrt{\text{Hz}}$

[a] From FEA simulation. [b] Standard deviation of ~20 000 measurements at 1 kHz. [c] Measured near the resonance (BW: 0.5 and 2 kHz for 406 and 210 μm long SMRs, respectively).

extensively demonstrated on micro- and nanocantilevers through standard fabrication techniques.[11,20–28] Doped single crystal silicon and polysilicon are advantageous as piezoresistive materials for micron-scale cantilevers since their gauge factors are much higher than those of metals which exclusively rely on geometric effects.[29] Furthermore, the gauge factor in doped semiconducting materials can be controlled *via* doping conditions such as impurity type and concentration.[30] Common fabrication methods for integrating piezoresistors onto silicon substrates include ion implantation, epitaxial growth, and diffusion from solid-source. Ion implantation is the preferred method for doping micrometer thick cantilevers, and is used here because it provides excellent control over doping concentration and dopant depth, and the implantation is straightforward to integrate with existing fabrication procedures.

SMR devices were fabricated at Innovative Micro Technology (Santa Barbara, CA) with a fusion-bonded silicon wafer with integrated microchannels, and two borosilicate glass wafers bonded to the top and bottom of the silicon wafer to form a gas tight package. Since most fabrication procedures are similar to those published previously,[13] only modified or newly developed steps are described herein. Prior to release of the cantilever from the silicon wafer, four ion implantation steps were added to create piezoresistors in the top silicon layer of the wafer stack (Innovion, Santa Barbara, CA). Background resistivity of the silicon wafer was approximately 1–20 Ω·cm (n-type). First a pre-implantation oxidation was performed for 10 minutes at 850 °C. Phosphorus ions were implanted at 160 keV with a dose of 1.0×10^{13} ions cm^{-2} to ensure consistent and uniform p–n junction isolation of the piezoresistors from the substrate. Then the wafer was annealed at 1050 °C for 10 hours under nitrogen. Boron ion implantations were performed at 50 keV with a dose of 5.0×10^{13} ions cm^{-2} for piezoresistors and at 120 keV with a dose of 5.0×10^{15} ions cm^{-2} for connections between the piezoresistors and the metal pads for wire-bonding. Finally phosphorus ions were implanted at 120 keV with a dose of 5.0×10^{15} ions cm^{-2} to form ohmic contacts between metal pads and the background silicon. Next the wafers underwent a second annealing under nitrogen at 950 °C for 1 hour. Junction depths for the piezoresistive and contact areas are approximately 0.5 and 1.2 μm, both of which are less than the top silicon layer thickness (~2 μm), ensuring electrical isolation from the fluid which could be conductive. In addition, doping levels in the piezoresistor and the surrounding n-well are sufficiently high to prevent full depletion on either side when the junction is reverse-biased. Resistivity of the piezoresistor becomes 0.04 Ω·cm after the second annealing. Besides bond pads, aluminium was selectively deposited on high boron-doped traces connecting the piezoresistor with the bond pads to further decrease the electrical resistance, except on areas for anodic bonding between the silicon wafer and the top glass wafer to ensure hermeticity.

Prior to anodic bonding, a 5000 Å plasma enhanced chemical vapor deposition (PECVD) oxide was deposited at 350 °C to protect the doped piezoresistors and contact areas from ionic contamination by sodium from the glass wafer.[31] The PECVD oxide was patterned and removed from the cantilever surface before the anodic bonding to minimize bending due to the mismatch of thermal expansion. Subsequent fabrication steps are identical to those for SMRs without piezoresistive readout.[13] The implanted piezoresistors are U-shaped but mostly parallel to the ⟨110⟩ direction to maximize the gauge factor for p-type dopants. The total resistor length is approximately 225 μm and measured electrical resistances are approximately 50 kΩ which is only 7% higher than estimated resistances for both 210 and 406 μm long SMRs. These two designs allow us to compare sensitivity of devices with different ratios of resistor length to cantilever length which are 0.5 and 0.26 for 210 and 406 μm long SMRs, respectively (see Table 1).

3. Experimental setup

Fig. 1 shows our experimental setup. For piezoresistive detection, a Wheatstone bridge is built with the piezoresistor and three external resistors. The bias voltage (~5 V) is selected to maximize the signal while limiting the temperature increase in the piezoresistor due to resistive heating. For optical-lever detection, a diode laser (635 nm) and a segmented photodiode are employed. The output signal from either the Wheatstone bridge or the photodiode is amplified, phase-shifted, and fed back to the actuator. Thus, the SMR always resonates at its resonance frequency through this feedback. To keep track of the resonance frequency of the SMR in real time, the output signal is heterodyne-mixed with a reference frequency from a function generator (33220A, Agilent) which is offset by ~1 kHz from the resonance frequency. The resulting signal is low-pass filtered ($f_c \approx 5$ kHz), converted to transistor–transistor logic levels, and measured with a frequency counter using a data acquisition card (NI PCI-6259, National Instruments).[12] Particles or cells travel through the microchannel *via* pressure-driven flow created by using pressure regulators and pneumatic valves. Detailed procedures and pressure settings used to control the bulk flow rate can be found elsewhere[12] (see Fig. 1 caption for typical pressure settings in each bypass channel). As shown in Fig. 1, the resonance frequency of the SMR decreases when a particle transits the suspended microchannel since the particle is denser than the surrounding fluid.

The SMR can either be actuated electrostatically by on-chip electrodes or acoustically by an off-chip piezoelectric crystal (PL022.31, Physik Instrument). Although optical-lever detection can maintain the feedback with either the electrostatic or piezocrystal actuation, piezoresistive detection with this generation of devices suffers from electrical coupling between the on-chip drive electrode and the piezoresistor which prevents operation in feedback-mode using electrostatic actuation. In order to make a meaningful comparison between the two detection schemes, off-chip piezocrystal actuation was used for all measurements.

4. Sample preparation

For mass sensitivity calibration, 4.17 μm diameter NIST size standard polystyrene beads (NT21N, Bangs Laboratories) were diluted with de-ionized water to a concentration of 1×10^7 particles mL^{-1}. For mixed particle measurement, NIST size standard polystyrene beads with the nominal diameter of 1.6, 2.0, 2.5, and 3.0 μm (4016A, 4202A, 4025A, and 4203A, Thermo Scientific) were diluted with de-ionized water and mixed to have a similar final concentration of 1×10^7 particles mL^{-1} for each bead. Budding yeast cells, *Saccharomyces cerevisiae*, were grown overnight at 23 °C in YEP (yeast extract plus peptone) media containing 2% glucose and 1 mg mL^{-1} adenine. The cultured yeast cells were then suspended and diluted with the same growth media to a concentration of approximately 1×10^7 cells mL^{-1}. Both the diluted particles and cells were sonicated for 1 min to break apart aggregates just before measurement.

5. Results and discussions

5.1 Heat transfer analysis

The SMR resonance frequency is sensitive to temperature which can be altered by heat produced in piezoresistive and optical-lever detection. For measurements of living cells, heat transfer analysis is important for ensuring that heat produced by the detection scheme does not significantly alter the temperature of the suspended microchannel. Finite element analyses (FEA) were used to estimate the temperature increase during SMR operation (see Table 1). To obtain a conservative estimate, the suspended

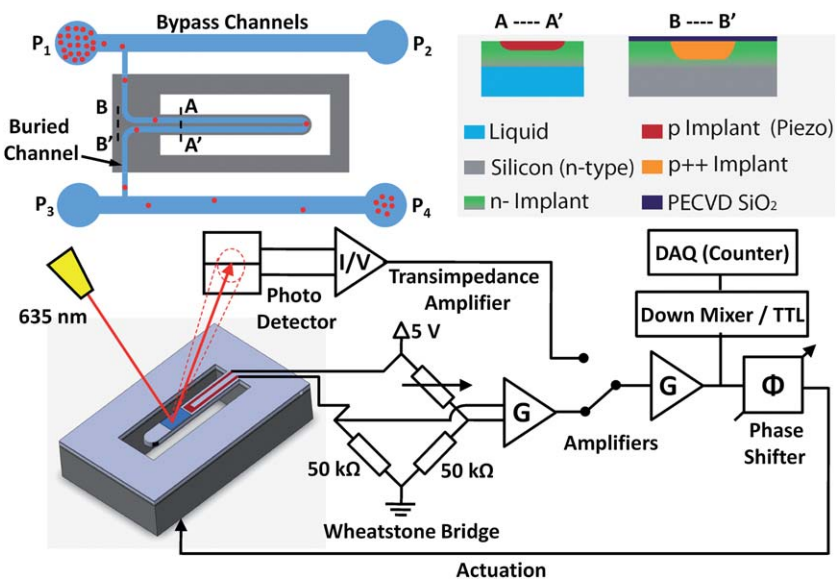

Fig. 1 Experimental setup for optical-lever and piezoresistive detection methods and interface to downstream electronics. The dynamic displacement of the SMR is measured with either the laser/photo-detector or the on-chip piezoresistor, amplified, phase-shifted, and fed back to a piezocrystal actuator. The resonance frequency is down-mixed to 1–2 kHz and recorded. Pressure settings are P_1 (15 psi) > P_2 (0 psi) and P_3 (15 psi) > P_4 (0 psi) for sample loading and P_1 (15 psi) = P_2 (15 psi) = P_3 (15 psi) and P_4 (variable, <15 psi) for population measurements.

microchannel was assumed empty since any fluid within the microchannel would only increase the thermal conductance. For typical experimental settings, the estimated maximum temperature increases for the piezoresistive detection due to Joule heating are 0.33 °C for both the 210 and 406 μm long SMRs, and maximum temperatures resulting from the optical-lever detection are 0.80 and 1.62 °C for 210 and 406 μm long SMRs, respectively. Since both 210 and 406 μm long SMRs have a piezoresistor with a fixed length located near the base, and the heat flux toward the tip is negligible due to the vacuum packaging, their thermal conductances are independent of the resonator length, and thus identical steady-state solutions are expected. In contrast, in optical-lever detection, heating occurs from absorption of the laser which is aligned near the tip of the resonator for optimal sensitivity. Thus, the thermal conductance decreases and the temperature estimate increases linearly with the length of the SMR. Overall, temperature increases resulting from either optical-lever or piezoresistive detection are not significant (within a few degrees Celsius).

5.2 Open loop frequency response

The amplitude and phase responses of the SMRs (see Fig. 2) are acquired by sweeping the frequency applied to the piezocrystal drive while measuring the sensor output with a lock-in amplifier (SR844, Stanford Research Systems). The frequency response is fitted to the model of a damped harmonic oscillator in order to determine the resonance frequency and quality factor. The resonance frequencies from optical-lever detection, for the device shown in Fig. 2, are slightly higher than those from piezoresistive detection by approximately 14 ppm (5.1 Hz) and 13 ppm (1.2 Hz), for 210 and 406 μm long SMRs, respectively. As expected, we see no significant difference in the quality factor measured with the two methods. Q-Values are lower than what we have observed with previous device generations due to the tall channel height and variability in the packaging process. Near the resonance frequency, the amplitude and phase responses are similar for both detection schemes. At frequencies away from the resonance frequency, the normalized amplitude and phase responses differ between optical-lever and piezoresistive detection for each SMR design. Although coupling exists in both detection schemes, deviation from the theoretical harmonic oscillator model is more pronounced using the piezoresistive detection scheme. This is due to parasitic capacitances between the piezoelectric actuator and piezoresistor together with its adjacent readout circuitry. Although these capacitances were significantly reduced by inserting a low impedance ground plane between the actuator and SMR, additional isolation will be necessary for eliminating it completely.

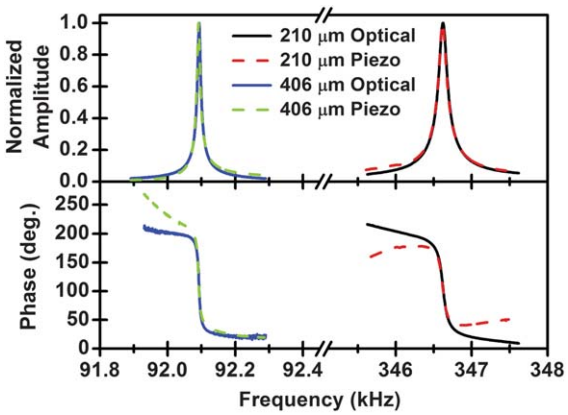

Fig. 2 Resonance responses for a 210 and a 406 μm long SMR measured with optical-lever and piezoresistive detection when each resonator is filled with de-ionized water. Parasitic coupling can be observed and is more apparent in the phase response. The extracted resonance frequencies for 210 and 406 μm long SMRs are 346 622.2 ± 0.6 Hz and 92 093.0 ± 0.1 Hz with optical-lever detection, and 346 617.3 ± 0.3 Hz and 92 091.8 ± 0.1 Hz with piezoresistive detection, respectively. The extracted quality factors for 210 and 406 μm long SMRs are 3647 ± 61 and 10 839 ± 77 with optical-lever detection and 3737 ± 14 and 10 872 ± 8 with piezoresistive detection, respectively.

5.3 Weighing particles

We have developed two different approaches for measuring the buoyant mass of individual particles with the SMR. For situations where precision is more desirable than throughput, vibrating the SMR at a large amplitude using strong excitation of the piezoelectric crystal creates an appreciable centrifugal force on a particle within the SMR. When the centrifugal force overcomes the viscous drag force, particles can be trapped near the U-turn of the SMR.[32] Fig. 3 shows the resonance frequency response as a single polystyrene bead from the 4.17 μm diameter NIST sample is trapped at the free end of the resonator. Alternatively, the inertial force can be reduced by attenuating the drive amplitude and particles can be weighed as they continuously flow through the SMR (see Fig. 4). Although the inertial trapping mode requires a slower flow velocity than the flow-through mode, which limits measurement throughput, the trapping mode provides higher precision because (i) SMR frequency stability in closed loop improves as the vibration amplitude increases, (ii) position-dependent error resulting from an uncertain channel crossing at the U-turn is eliminated, and (iii) longer averaging times are possible. As can be observed in Fig. 3 and 4, the frequency response for both detection modes is similar for each SMR design, demonstrating that the detection scheme does not alter the mass sensitivity. Approximately 1000 beads were measured using each device type, and average mass sensitivities were −5.42 and −0.74 Hz pg^{-1} for 210 and 406 μm long SMRs, respectively (negative mass sensitivities indicate downshift of the resonance frequency upon mass loading). These measured sensitivities show good agreement with theoretical estimates (see Table 1).

In Fig. 5 we demonstrate buoyant mass measurements of a mixture of polystyrene beads and yeast cells with the piezoresistive detection in the flow-through mode. The mean buoyant mass of each bead extracted from the measured mass histogram is linear with mean volume from manufacturer specification, as expected (adjusted R^2 = 0.99999, inset). Mass density of the polystyrene extracted from the slope in the linear regression is 1.047 g cm^{-3} which is comparable to the manufacturer specification (1.05 g cm^{-3}). Coefficients of variation in buoyant mass are 3.28, 2.34, 2.27, and 1.86% for 1.6, 2.0, 2.5, and 3.0 μm bead samples, respectively, which are generally better than the coefficients of variation in volume provided by the manufacturer (3.90,

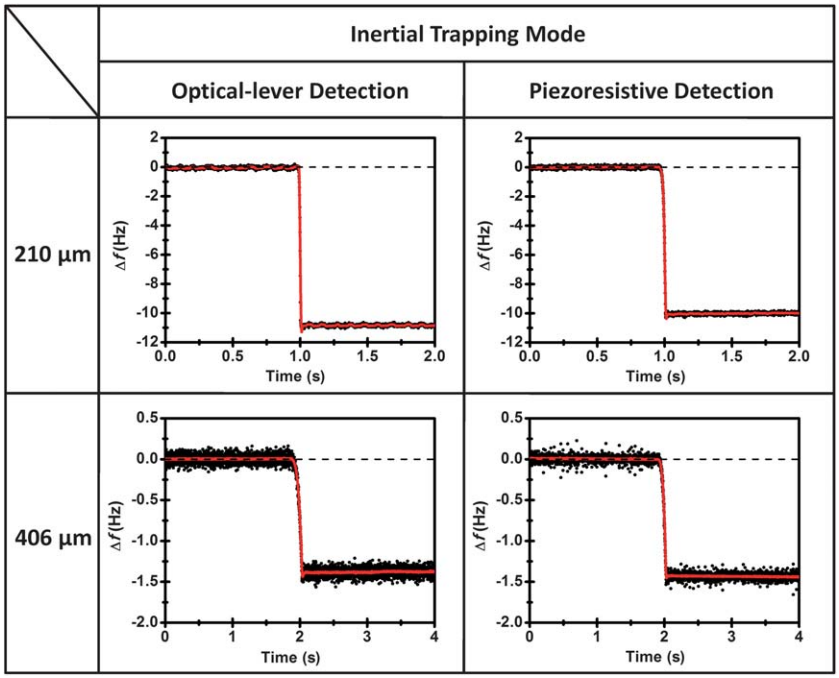

Fig. 3 Frequency response during a single particle inertial trapping event (4.17 µm diameter polystyrene bead in deionized water) as measured by optical-lever and piezoresistive detection. Frequency is measured at a sampling rate of 1 kHz (black dots) and smoothed (red line) with a Savitzky–Golay filter (3rd order, $n = 50$).

3.00, 3.00, and 3.30% for 1.6, 2.0, 2.5, and 3.0 µm bead samples, respectively). As expected, the buoyant mass histogram for budding yeast cells is wider than particle mass histograms. The wider distribution results from budding yeast's asymmetric division and consequential variation in growth rate.[33,34]

5.4 Frequency noise and mass resolution

Although mass sensitivity, *i.e.* the frequency shift caused by a given mass change, is independent of the readout method, piezoresistive and optical detection are expected to provide

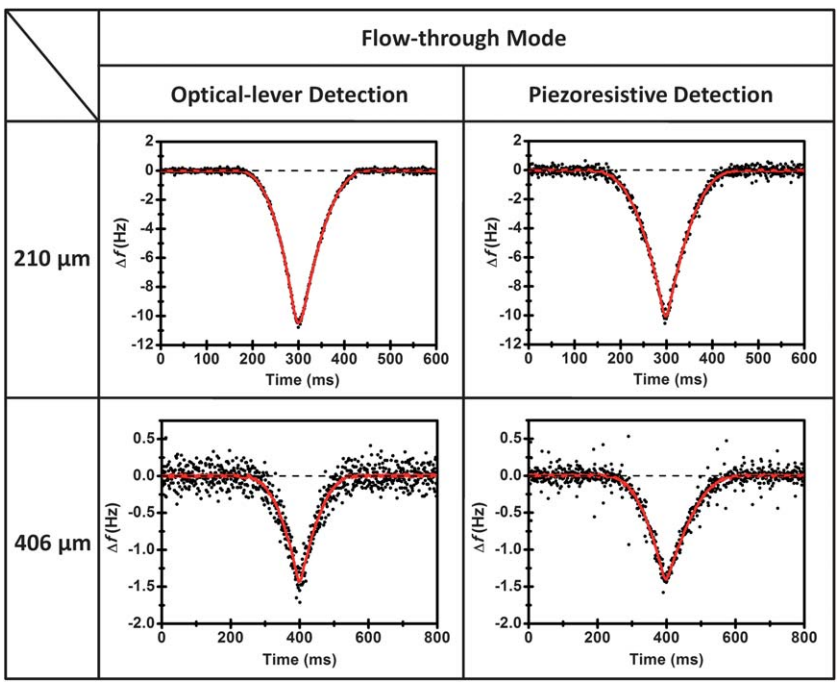

Fig. 4 Frequency response during the passage of a single particle (4.17 µm diameter polystyrene bead in deionized water) as measured by optical-lever and piezoresistive detection. Inertial trapping, as shown in Fig. 3, was eliminated by adding a 20 dB attenuator between the piezoelectric crystal and the feedback circuit. Frequency is measured at a sampling rate of 1 kHz (black dots) and smoothed (red line) with a Savitzky–Golay filter (3rd order, $n = 25$).

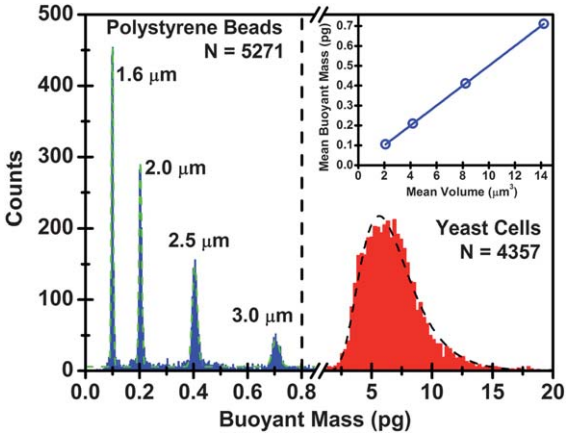

Fig. 5 Buoyant mass histograms of mixed polystyrene beads (left) and yeast cells (right) measured with piezoresistive detection. Mixed polystyrene beads (1.587 ± 0.025, 1.998 ± 0.022, 2.504 ± 0.025, and 3.005 ± 0.027 μm diameter beads) are measured with 210 μm long SMR and yeast cells are measured with 406 μm long SMR. Both measurements are made at room temperature. Inset shows mean buoyant mass is linear to mean volume. Histogram for bead mixtures is fitted to multi-peak Gaussian (dashed green line) and histogram for yeast cells is fitted to log-normal (dashed black line).

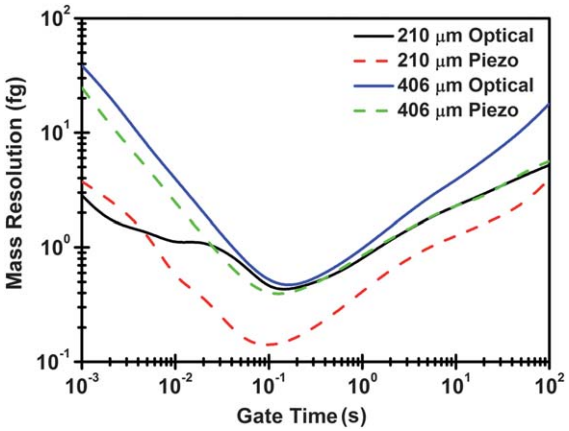

Fig. 6 Mass resolution derived from sensitivity calibration and measured Allan variance of the SMR resonance frequency of SMRs as a function of the gate time, which is an averaging window for Allan variance calculation. Raw data were measured at a sampling rate of 1 kHz for 1 hour.

different mass resolutions due to the different characteristics of their frequency noise. To determine mass resolution of the SMRs, frequency noise was measured and analyzed for each SMR type with both detection schemes (see Table 1). Standard deviations of the resonance frequency measured for 20 seconds at a sampling rate of 1 kHz with the optical-lever were 44 and 207 ppb for the 210 and 406 μm long SMRs, respectively. With the same measurement conditions, standard deviations measured with the piezoresistive detection were 54 and 146 ppb for the 210 and 406 μm long SMRs, respectively. To obtain the above frequency noise levels, the maximum drive amplitude was applied to the piezoelectric crystal, causing particles to be trapped *via* the inertial trapping mode described previously. In addition, the optical-lever was well aligned and the piezoresistor operation was optimized relative to the settings used in previous sections. Specifically, a lower amplifier gain and higher bias voltage to the Wheatstone bridge (up to ~11 V which increases the maximum temperature to ~1.60 °C; this temperature is slightly higher than and comparable to the optical-lever for 210 and 406 μm long SMRs, respectively) and the phase shift were adjusted carefully to obtain maximum frequency stability. Among these optimization parameters, the effect of phase adjustment is the most critical. Mass resolution of the 210 μm long SMR with the optical-lever is 2.8 fg, slightly better than 3.4 fg measured with the piezoresistor. However, mass resolution of the 406 μm long SMR with the piezoresistor is 18.1 fg, better than 25.8 fg measured with the optical-lever.

To investigate the long-term frequency stability, frequency noise was measured for 1 hour at a sampling rate of 1 kHz and analyzed with Allan variance.[35] Fig. 6 shows mass resolution derived from mass sensitivity and Allan variance. Mass resolutions at the gate time of 1 ms agree with ones from standard deviations for short-term (20 s) measurements. More interestingly, mass resolution improves by at least one order of magnitude from gate times of 1 ms to ~100 ms for each SMR type and detection scheme. Piezoresistive detection with the 210 μm long SMR offers the best mass resolution of 135 ag at ~100 ms which is 3-fold better than optical-lever detection with the same SMR type. This suggests that piezoresistive detection with a longer gate time can increase the mass resolution for applications that can tolerate the reduced temporal resolution. At 1 ms, Allan variances resulting from thermomechanical noise[36] are 6.2×10^{-19} and 6.1×10^{-18} for the 210 and 406 μm long SMRs both of which are 4 orders of magnitudes better than the best measurement for each SMR type. Allan variance due to thermomechanical noise monotonically decreases with increasing gate time as expected. Measured Allan variances, however, exhibit a crossover between the two detection schemes as well as minima, after which the variances increase. Low frequency instabilities observed may result from noise due to the transducer itself ($1/f$ noise) and downstream feedback electronics.

Since the frequency noise is expected to be related to the displacement noise, we used a Laser Doppler Vibrometer (LDV) to calibrate the sensor response. This was accomplished by using the piezoelectric actuator to resonate the SMR with various drive voltage amplitudes while the SMR tip amplitude was measured by the LDV (OFV 511 with OFV 3001, Polytec). Optical and piezoresistive readouts were recorded at each drive amplitude in order to obtain a calibration figure. For the optical-lever, the LDV calibration showed reasonable agreement with calibration using the thermomechanical spectra.[27] Optical-lever sensitivities from LDV measurements were 49 and 43% lower than those from thermomechanical spectra for 210 and 406 μm long SMRs, respectively. However, the piezoresistor could not resolve the thermomechanical spectra due to the Johnson noise limited sensitivity. Instead, LDV calibration for the piezoresistor was validated by theoretical estimates using FEA. When the attenuation due to parasitic impedances originating from the Wheatstone bridge and coaxial cables is considered,[37] the measured and estimated sensitivity agreed within a factor of two (Piezoresistor sensitivities from LDV measurements were 18 and 47% lower than those from FEA for 210 and 406 μm long SMRs,

respectively). Using LDV calibration results, the voltage noise near the resonance of each detection method measured by a spectrum analyzer (4395A, Agilent) could be converted into displacement noise (see Table 1). Interestingly, the displacement noise of piezoresistive detection is two orders of magnitude higher than that of the optical detection for each SMR type. Given that the frequency noise is comparable, this unexpected finding suggests that properties associated with the self-excited feedback operation may govern the overall performance in our system.

6. Conclusions and future outlook

We have developed suspended microchannel resonators with electronic readout by integrating doped silicon piezoresistive elements with the resonators. The fabricated devices are characterized for both optical-lever and piezoresistive detection using external piezocrystal actuation. For inertial trapping mass sensing applications, the piezoresistive detection offers mass resolution on the order of a few femtograms in a 1 kHz bandwidth which is on the same order of magnitude as that of optical-lever detection. We successfully implemented the piezoresistive detection scheme to measure buoyant mass histograms of a mixture of NIST size standard particles and budding yeast cells. We envision that eliminating the need for optical components will enable new uses for the SMR in both multiplexed and field deployable applications.

Acknowledgements

This work was supported by the Institute of Collaborative Biotechnologies through contract no. W911NF-09-D-0001 from the US Army Research Office and the NIH Cell Decision Process Center P50-GM68762. T.P.B. gratefully acknowledges funding by the Max Planck Society and the MPI for Biophysical Chemistry.

Notes and references

1 H. J. Butt, *J. Colloid Interface Sci.*, 1996, **180**, 251–260.
2 C. A. Savran, S. M. Knudsen, A. D. Ellington and S. R. Manalis, *Anal. Chem.*, 2004, **76**, 3194–3198.
3 R. Berger, E. Delamarche, H. P. Lang, C. Gerber, J. K. Gimzewski, E. Meyer and H.-J. Güntherodt, *Science*, 1997, **276**, 2021–2024.
4 G. H. Wu, H. F. Ji, K. Hansen, T. Thundat, R. Datar, R. Cote, M. F. Hagan, A. K. Chakraborty and A. Majumdar, *Proc. Natl. Acad. Sci. U. S. A.*, 2001, **98**, 1560–1564.
5 J. Zhang, H. P. Lang, F. Huber, A. Bietsch, W. Grange, U. Certa, R. McKendry, H.-J. Güntherodt, M. Hegner and C. Gerber, *Nat. Nanotechnol.*, 2006, **1**, 214–220.
6 A. Gupta, D. Akin and R. Bashir, *Appl. Phys. Lett.*, 2004, **84**, 1976–1978.
7 K. Y. Gfeller, N. Nugaeva and M. Hegner, *Biosens. Bioelectron.*, 2005, **21**, 528–533.
8 B. Ilic, D. Czaplewski, M. Zalalutdinov, H. G. Craighead, P. Neuzil, C. Campagnolo and C. Batt, *J. Vac. Sci. Technol., B*, 2001, **19**, 2825–2828.
9 G. Meyer and N. M. Amer, *Appl. Phys. Lett.*, 1988, **53**, 1045–1047.
10 P. K. Hansma, B. Drake, D. Grigg, C. B. Prater, F. Yashar, G. Gurley, S. V. Eling, S. Feinstein and R. Lal, *J. Appl. Phys.*, 1994, **76**, 796–799.
11 M. Tortonese, R. C. Barrett and C. F. Quate, *Appl. Phys. Lett.*, 1993, **62**, 834–836.
12 T. P. Burg, M. Godin, S. M. Knudsen, W. Shen, G. Carlson, J. S. Foster, K. Babcock and S. R. Manalis, *Nature*, 2007, **446**, 1066–1069.
13 M. Godin, A. K. Bryan, T. P. Burg, K. Babcock and S. R. Manalis, *Appl. Phys. Lett.*, 2007, **91**, 123121.
14 T. Sulchek, R. J. Grow, G. G. Yaralioglu, S. C. Minne, C. F. Quate, S. R. Manalis, A. Kiraz, A. Aydine and A. Atalar, *Appl. Phys. Lett.*, 2001, **78**, 1787–1789.
15 S. H. Lim, D. Raorane, S. Satyanarayana and A. Majumdar, *Sens. Actuators, B*, 2006, **119**, 466–474.
16 M. Li, W. H. P. Pernice and H. X. Tang, *Nat. Nanotechnol.*, 2009, **4**, 377–382.
17 O. N. Tufte, D. Long and P. W. Chapman, *J. Appl. Phys.*, 1962, **33**, 3322–3327.
18 K. D. Samaun, J. B. Wise and J. B. Angell, *IEEE Trans. Biomed. Eng.*, 1973, **BME–20**, 101–109.
19 A. Partridge, J. K. Reynolds, B. W. Chui, E. M. Chow, A. M. Fitzgerald, L. Zhang, N. I. Maluf and T. W. Kenney, *J. Microelectromech. Syst.*, 2000, **9**, 58–66.
20 Y. Su, A. G. R. Evans, A. Brunnschweiler, G. Ensell and M. Koch, *Sens. Actuators, A*, 1997, **60**, 163–167.
21 T. Gotszalk, J. Radojewski, P. B. Grabiec, P. Dumania, F. Shi, P. Hudek and I. W. Rangelow, *J. Vac. Sci. Technol., B*, 1998, **16**, 3948–3953.
22 B. W. Chui, T. D. Stowe, Y. S. Ju, K. E. Goodson, T. W. Kenny, H. J. Mamin, B. D. Terris, R. P. Ried and D. Rugar, *J. Microelectromech. Syst.*, 1998, **7**, 69–78.
23 J. Thaysen, A. Boisen, O. Hansen and S. Bouwstra, *Sens. Actuators, A*, 2000, **83**, 47–53.
24 P. A. Rasmussen, J. Thaysen, S. Bouwstra and A. Boisen, *Sens. Actuators, A*, 2001, **92**, 96–101.
25 B. L. Pruitt and T. W. Kenny, *Sens. Actuators, A*, 2003, **104**, 68–77.
26 I. Bargatin, E. B. Myers, J. Arlett, B. Gudlewski and M. L. Roukes, *Appl. Phys. Lett.*, 2005, **86**, 133109.
27 M. Li, H. X. Tang and M. L. Roukes, *Nat. Nanotechnol.*, 2007, **2**, 114–120.
28 J. Lee and W. P. King, *J. Microelectromech. Syst.*, 2008, **17**, 432–445.
29 G. Ensell, S. P. Beeby, M. Kraft and N. White, *MEMS Mechanical Sensors*, Artech House, Boston, 2004.
30 Y. Kanda, *IEEE Trans. Electron Devices*, 1982, **29**, 64–70.
31 K. Schjolberg-Henriksen, G. U. Jensen, A. Hanneborg and H. Jakobsen, *J. Micromech. Microeng.*, 2003, **13**, 845–852.
32 J. Lee, W. Shen, K. Payer, T. P. Burg and S. R. Manalis, *Nano Lett.*, 2010, **10**, 2537–2542.
33 L. H. Hartwell and M. W. Unger, *J. Cell Biol.*, 1977, **75**, 422–435.
34 C. L. Woldringh, P. G. Huls and N. O. E. Vischer, *J. Bacteriol.*, 1993, **175**, 3174–3181.
35 D. W. Allan, *Proc. IEEE*, 1966, **54**, 221.
36 A. N. Cleland and M. L. Roukes, *J. Appl. Phys.*, 2002, **92**, 2758–2769.
37 In the existing setup, the cable lengths and amplifier type contribute a total capacitance of ~166 pF. With a piezoresistor resistance of ~50 kΩ, a first-order low-pass filter is created with a pole at ~25 kHz. This low-pass filtering effect contributes 24 and 14 dB attenuation for the 210 and 406 μm long SMR, respectively.